**Methods**

Nikola Fischer*, Johannes Knapp* and Franziska Mathis-Ullrich

# Shape-sensing by self-sensing of shape memory alloy instruments for minimal invasive surgery

Inherente Formerkennung von Formgedächtnis Instrumenten für die minimalinvasive Chirurgie

https://doi.org/10.1515/auto-2023-0058
Received April 12, 2023; accepted May 31, 2023

**Abstract:** Shape memory alloy-based flexible instruments have potential for enhancing the safety in minimally invasive surgery compared to passive rigid devices. We developed a data-driven polynomial model to estimate deflection of a 2D bending actuator using electrical resistance. The model accurately predicts deflections (mean error <3.6 mm), but force sensing augmentation is required for unknown load cases. The model is specific to the tested actuator geometry, and future research should investigate multiple actuators and explore nonlinear modeling approaches.

**Keywords:** data-driven modeling; MIS; nickel-titanium; polynomial modeling; SMA

**Kurzfassung:** Flexible Instrumente aus Formgedächtnislegierungen können in der minimalinvasiven Chirurgie eingesetzt werden, um die Sicherheit des Eingriffes im Vergleich zu starren unbeweglichen Instrumenten zu erhöhen. Mit einem datengetriebenen Polynommodell kann die Formveränderung eines 2D-Biegeaktors mithilfe des elektrischen Widerstandes geschätzt werden. Die Bestimmung der Biegung mit einem mittleren Fehler von <3.6 mm war damit möglich. Für unbekannte Lastfälle ist jedoch eine zusätzliche Kraftmessung erforderlich. Zukünftige Arbeiten sollten die Generalisierung hinsichtlich verschiedener Aktuatoren und nichtlineare Modellierungsansätze untersuchen.

**Schlagwörter:** datengetriebene Modellierung; MIC; Nickel-Titan; Polynom Modell; Formgedächtnislegierung

Nikola Fischer and Johannes Knapp contributed equally to this work.

***Corresponding authors: Nikola Fischer and Johannes Knapp**, Institute for Anthropomatics and Robotics (IAR) at Karlsruhe Institute of Technology (KIT), 76131 Karlsruhe, Germany, E-mail: nikola.fischer@kit.edu (N. Fischer), johannes.knapp@kit.edu (J. Knapp). https://orcid.org/0000-0001-9364-3328 (N. Fischer)
**Franziska Mathis-Ullrich**, Department Artificial Intelligence in Biomedical Engineering (AIBE) at Friedrich-Alexander University Erlangen-Nürnberg (FAU), 91052 Erlangen, Germany,
E-mail: franziska.mathis-ullrich@fau.de

## 1 Introduction

### 1.1 Motivation

Minimally invasive surgery (MIS) is a type of surgical procedure that involves small incisions and specialized surgical instruments to perform medical procedures. Compared to traditional surgery, MIS has several benefits for patients, medical experts, and hospitals. One of the main advantages of MIS is that it is less traumatic for patients due to smaller incisions, with the consequence of reduced risk of complications such as infections and bleeding [1]. This leads to less pain and discomfort for patients, and thus to a shorter recovery time and less scarring [2].

Flexible instruments in particular can be useful in MIS because they provide greater maneuverability and access to hard-to-reach areas within the body in comparison with rigid instruments, while reducing the risk of injury to surrounding tissue and organs. While passive flexible instruments (e.g., steerable needles) deform due to interaction with tissue only, active flexible instruments provide in addition an actuation that allows to change their shape.

Shape memory alloys (SMAs) (e.g. nickel-titanium) are *smart materials* that autonomously find back into a preset original shape when undergoing a crystalline phase transition from martensite to austenite due to temperature changes. This effect is referred to as the *shape memory effect* and can be utilized in a flexible instrument to obtain multiple segments with individual actuation [3].

Despite the useful dexterity of a flexible instrument based on SMAs, their control within the human body remains challenging. The shape of the instrument within the body cavity depends on various influencing factors. Those factors are mainly the applied force at the external (proximal) end of the instrument, the mechanical property of the surrounding tissue, and the temperature of the SMA. Visual imaging devices (e.g., endoscopic cameras) that monitor the

flexible instrument and the site of operation are thus crucial for clinicians to manipulate the instrument effectively. However, ideal imaging is not always provided during a medical procedure due to the lack of additional endoscopic devices, limited access into the confined space, or an impaired line of sight caused by body fluids and smoke.

For this reason, additional intraoperative information about the shape and the pose of the instrument's distal tip are highly beneficial to the operator. Due to the confined space in the cavity and the compactness of the delicate instruments themselves, attaching and operating additional sensor technology (e.g., resistance based flex sensors [4], fiber grading sensors [5]) is often hardly feasible. Instead, flexible instruments with inherent actuation such as SMAs could use the structural material for both, actuating and sensing. They not only provide intrinsic actuation once heated, but also present a variability of their electrical resistance (ER) in accordance with the change of their shape (i.e., self-sensing) [6].

The change of the ER as an intrinsic property has been utilized in research in order to determine the strain of a nickel-titanium alloy wire, e.g., Ikuta et al. [7] and Prechtl et al. [8]. Kaiser et al. have developed measurement and control electronics to use a microcontroller to heat a SMA using electric current and measure the ER [9], while Ma et al. implemented the control of a lengthening SMA wire using a neural network [10]. Furthermore, grasping applications driven by SMA wire actuators were investigated by Wang et al. who controlled the deformation of a flexible gripper to grasp deformable objects [11]. Since the ER changes as a function of the wire strain, a control based on self-sensing could be demonstrated. In addition, Lan et al. were able to control the position of the tip of a flexible micro-gripper [12]. They used a spring to elongate a SMA wire and forced it to contract by electric current (i.e., Joule heating). The authors followed the approach of length control further and investigated a data-driven approach using a polynomial model [13].

### 1.2 Contribution

Previous research has predominantly focused on investigation of one-dimensional strain variations of SMAs and has even demonstrated controlled actuation for defined loading conditions based on electrical resistance. However, the potential of SMAs to perform complex three-dimensional shape changes has not been fully explored, even though such flexibility could be highly beneficial in the design of minimally invasive surgical instruments to reach further within confined spaces. This work presents a proof-of-concept modeling approach that correlates the electrical resistance of a simplified SMA-based actuator with its shape, enabling two-dimensional shape changes in novel smart minimally invasive instruments (see Figure 1).

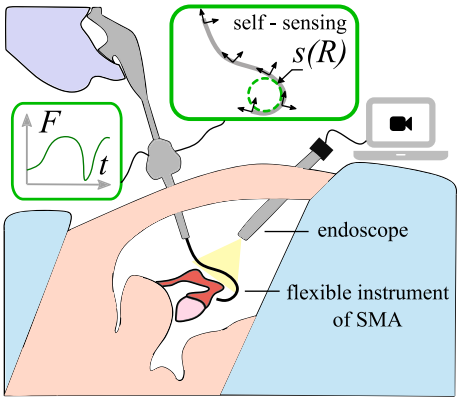


**Figure 1:** Vision of a minimally invasive surgery (MIS) with a flexible instrument made of a shape memory alloy (SMA). Augmenting the video endoscopy with information about deflection $s$ and interaction forces $F$.

## 2 Methods

A simplified actuator with inherent SMA actuation was fabricated and investigated in an experimental setup for multiple actuation cycles in different load-heat scenarios while recording various system parameters. Thus, a data-driven polynomial model could be designed which was able to estimate the actuator's shape.

### 2.1 SMA actuator

For the actuator, we use a nickel-titanium-copper (NiTiCu) wire (Ø 0.7 mm, 230 mm long). Nickel and titanium form the basic components for an alloy with shape memory effect. By adding copper, characteristics can be adjusted, such as the transformation temperatures, i.e. austenite

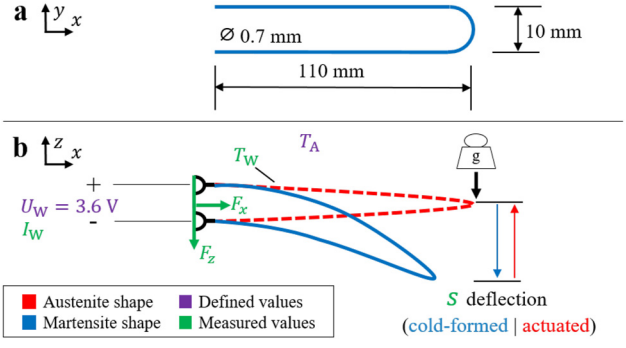


**Figure 2:** Simplified actuator design with a flat U-shaped wire from NiTiCu (a). Schematic of the shape changes between martensite (blue) and austenite states at $A_f = 65\,°C$ (red). Known parameters include power supply voltage $U_W$, ambient temperature $T_A$, and load. Current $I_W$, force $F$, deflection $s$, and wire temperature $T_w$ are measured during the experiments.

starting temperature $A_s$ and austenite finish temperature $A_f$, as well as the hysteresis of the temperature-shape correlation [14]. The wire is then bent into a plane U-shaped loop with a bending radius at the tip of 5 mm (see Figure 2a). This shape is first cold-formed and then "imprinted" (i.e. shape-setting) by heating it to 425 °C and keeping it at that temperature for 30 min [15]. Afterwards it is quenched in water (<25 °C).

This basic straightened (austenite) shape can be cold-formed (i.e. bent) under an external load. If the bent wire is then heated above the austenite finish temperature (here: $A_f = 65$ °C), the original straight austenite form is restored (see Figure 2b). This effect of SMAs can be used to apply mechanical forces [16]. The aforementioned design allows to power the instrument at its proximal end, using Joule heating to increase the temperature of the wire, thus avoiding an interference of cable and connectors at the instrument's body.

## 2.2 Experimental setup

The defined and measured values are schematically illustrated in Figure 2b. The inherent electric resistance of the wire $R$ can be defined as

$$R = \frac{U_W}{I_W} \tag{1}$$

where $U_W$ is the voltage applied at the proximal wire ends and $I_W$ the electric current in the wire. Further experimental parameters of interest include the wire surface temperature $T_W$, the deflection $s$ at the distal tip, as well as the applicable distal force $F$. The experimental setup is shown in Figure 3. The SMA actuator is mounted horizontally with its two proximal ends in a fixed clamp. In the unloaded state, the tip of the wire is aligned approximately at the horizontal level of the clamping. The actuator can be powered via the clamped wire ends and its temperature will increase due to Joule heating. This allows to trigger a phase transformation from various cold-formed shapes back into the set horizontal austenite shape.

The electronics to power the wire and record the measurement data at the same time are controlled by a microcontroller (Arduino Uno Rev3 SMD). To measure the current $I_W$ at a given voltage $U_W$, a measuring resistor (Isabellenhütte PBV R010, Germany) is used. Two operational amplifier circuits (Texas Instruments TLC 2272, USA) are implemented to amplify the voltage drops at the measuring resistor and the SMA wire. Then, $R$ can be calculated with (1). The setup provides the restistance $R$ of the SMA wire with a resolution of 1 mΩ and an accuracy of 3 mΩ.

To measure the force components of $F = [F_x, F_z]$ on the wire clamping, two load cells with measuring amplifier (Sparkfun Electronics TAL221, HX711, USA) are used. The signals are calculated and processed by the microcontroller and transmitted via Serial connection to a host computer. In the heating phase, $F$ and $R$ values are measured with a frequency of up to 385 Hz, limited by the electronic evaluation system of the load cells. Data acquisition in the cooling phase is conducted with 1.75 Hz due to fact that $R$ could only be measured when current flows through the actuator. Consequently, the current rate must be kept at a minimum during cooling phase to avoid additional unintended Joule heating.

We developed a measurement script in Python (3.9) to track the position of the wire tip with an ArUco marker and a visual camera (Intel Corporation RealSense™ D435, USA), as well as to compute and store the position data. Preliminary tests revealed a marker tracking position accuracy of 0.2 mm. A thermal imaging camera (Teledyne FLIR LLC FLIR E60, USA) is used for contactless temperature monitoring of the wire surface $T_W$. The ambient temperature $T_A$ is the constant room temperature (22.5 °C) of the laboratory and is monitored with an additional sensor. The temperature fluctuation remained within a range of 2 °C.

To bend the actuator at ambient temperature, weights are attached to the actuator's distal tip. The load pulls the tip down in negative $z$ direction. If the actuator is then powered, the shape memory effect "opposes" the shape change and lifts the weight. When the power is turned off and the temperature decreases, the wire again deforms by the gravitational force of the weight.

The generalized deflection $s$ is utilized as a simplified measure of the bent shape of the wire (see Figures 2 and 4). In this work, $s$ corresponds to $z$. It should be noted, that due to many past actuation cycles of the actuator ($n > 300$), a two-way shape memory effect was observed [17]. The bent shape in martensite phase had become part of the material's memory. Thus, the bent shape was obtained even in cases without any load. This way, a common starting point between $s = -138$ mm (unloaded) and $s = -143$ mm (100 g) is provided for both cases, with and without load.

## 2.3 Training data acquisition

Load cases were defined for data acquisition in order to subsequently fit a polynomial model. In a load case, a specific weight and heating period are defined. Weights were applied in the range from 0 g to 100 g

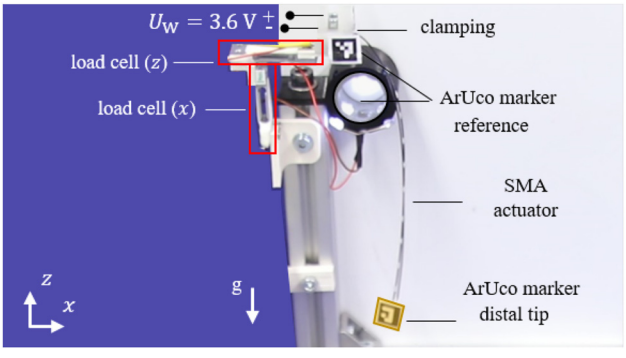


**Figure 3:** Experimental setup for data acquisition of the SMA actuator. Two load cells (red) record reaction forces $F_x$ and $F_z$ at the clamping. Tracking ArUco markers at the clamping and the distal tip (yellow) allow to measure the deflection $s$.

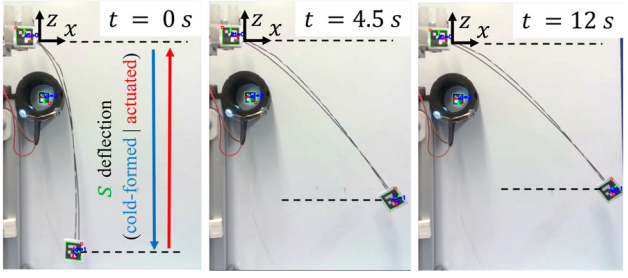


**Figure 4:** Actuator bending shape at 0 s, 4.5 s and 12 s. A visible deflection of the distal tip over an actuation period of 0 s–12 s can be observed.

in 10 g steps. Preliminary tests revealed a maximum possible heating period of 12 s at 3.6 V, avoiding over-heating and damage to the setup. The heating period was set accordingly.

The experimental procedure of an actuation cycle started for each case with the loading of the actuator at ambient temperature $T_A$ (i.e. in martensite state). This leads to a deflection of the distal tip from the initial horizontal position. Then, a voltage of 3.6 V was applied by a laboratory power supply to re-obtain the horizontal straight shape (see Figure 4). Data were recorded for 240 s from the start of heating. This procedure was repeated twice without resetting the actuator load-free to the horizontal shape. The overall training data thus included 22 experimental training cycles, namely 2 trials for each of the 11 weights. The typical hysteresis of deflection $s$ and resistance $R$ of an example actuation cycle is shown in Figure 5. Maximum temperatures on the actuator surface remained <80 °C during our investigations (see Figure 6).

## 2.4 Polynomial modeling

A polynomial approach was chosen for the shape estimation since it allows in a simple manner to represent a nonlinear relationship of the measurement in several dimensions. Our model was developed in MATLAB 2021b and should estimate the vertical deflection of the actuator tip $\hat{s}$ based on the measured input parameters of the resistance $R$, the vertical force at the clamping $F_z$, and the heating status, schematically shown in Figure 7. The force data is required in addition to the resistance to cover medical use cases of arbitrary unknown interaction forces between instrument and tissue. Only $F_z$ was considered as preliminary tests revealed it as the dominant force component

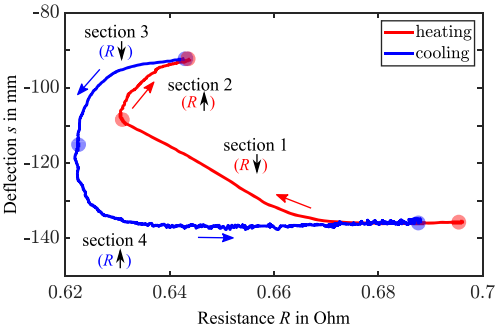


**Figure 5:** Measured resistance $R$ and deflection $s$ for no load of a full actuation cycle of the actuator including heating (red) and cooling phase (blue). Colored arrows indicate the chronicle order of Sections 1–4, subdividing the actuation cycle into four polynomial submodels, based on whether the resistance $R$ increases or decreases. Semi-transparent circles denote the transitions between sections.

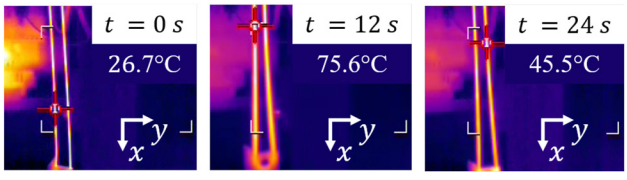


**Figure 6:** Actuator surface temperature during an actuation cycle. Heating period was set to 12 s, followed by a (passive) cooling phase for the remaining 228 s of data recording. Every trial started at $T_W < 27$ °C.

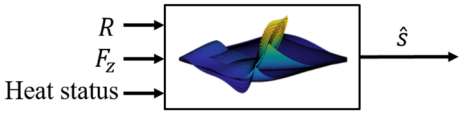


**Figure 7:** Schematic of the polynomial model with the input variables of resistance $R$, force $F_z$ and heat status. The output is a deflection estimate $\hat{s}$.

for the investigated load cases. The general representation of the two-dimensional-polynomials can be written as

$$\hat{s} = \sum_{i=0}^{M_R} \left( \sum_{j=0}^{N_F} \left( p_{ij} \cdot R^i \cdot F_z^j \right) \right) \tag{2}$$

where $i$ and $j$ indicate the power of $R$ and $F_z$ with the coefficient $p_{ij}$. $M_R$ and $N_F$ indicate the highest degree of the polynomial in the dimension $R$ and $F_z$, respectively.

The polynomials were fitted to the data with the *rmse* function minimizing the root-mean-square error $Q$ defined as

$$Q = \sqrt{\frac{1}{N_{\text{data}}} \sum_{k=1}^{N_{\text{data}}} (\hat{s} - s)^2} \tag{3}$$

where $\hat{s}$ denotes the estimated value, $s$ the actual measured value, and $N_{\text{data}}$ is the number of measurement points during data acquisition. Since the relationship between $R$ and $s$ is characterized by a hysteresis depending on heating and cooling phases, the actuation cycle is subdivided. In contrast to Lan et al. [13], the hysteresis was not reduced to one single polynomial. Instead, four separate polynomials were fitted for the four different sections, thus covering the hysteresis entirely (see Figure 5). Each section can be distinguished based on heating status (i.e. heating, cooling) and the resistance $R$ (i.e. increasing, decreasing) and thus be modeled by a separate polynomial. For real time estimation, the model compares the actual measured resistance value to the last measured values. Based on the heating status and the behavior of the electrical resistance, the model estimates the deflection within the corresponding section. In Table 1 the computed coefficients $p_{ij}$ are listed.

## 2.5 Model evaluation

For the purpose of model evaluation, further experiments were conducted to test the model for three simplified application scenarios, as shown in Figure 8. Those include the actuation against no resistance i.e. 0 g load (Figure 8a), small resistance i.e. 20 g load (Figure 8b), and a blocking resistance occurring at 50 % of maximum deflection (Figure 8c), which corresponds to $s \approx -116$ mm.

In addition, the heating period for each scenario was varied. Besides the maximum heating period of 12 s representing a full actuation cycle, also shorter heating periods must be considered. In medical use cases, flexible instruments might be actuated to transform into intermediate shapes between initial and maximum deflection. Therefore, the heating period of 4.5 s was also tested. In a third variation, we simulated a repetitive readjustment of the shape with a short heating period of 4.5 s, a 7.5 s cooling break, followed by another 6 s long heating period. Thus, for the evaluation, 9 different load-heat scenarios were conducted with 2 experimental trials, each.

Figure 9 presents the quantitative evaluation procedure schematically. The estimated deflection $\hat{s}$ of the wire was subsequently

**Table 1:** Coefficients for the two-dimensional polynomial model.

| | Section 1 | Section 2 | Section 3 | Section 4 |
|---|---|---|---|---|
| | $M_R = 4$<br>$N_F = 3$ | $M_R = 2$<br>$N_F = 4$ | $M_R = 3$<br>$N_F = 5$ | $M_R = 5$<br>$N_F = 4$ |
| p00 | −3.298e+05 | −3.907e+04 | −1.86e+06 | 7.809e+06 |
| p01 | −4.525e+04 | 7.412e+04 | 5.202e+06 | −8.168e+05 |
| p02 | 8732 | −3.771e+04 | −3.158e+06 | 8.456e+04 |
| p03 | −903.2 | −9.15e+04 | 1.937e+04 | −1.027e+04 |
| p04 | – | – | 7605 | 231.4 |
| p05 | – | – | −636.9 | – |
| p10 | 2.048e+06 | 1.213e+05 | 8.762e+06 | −5.79e+07 |
| p11 | 1.83e+05 | −2.314e+05 | −2.455e+07 | 4.761e+06 |
| p12 | −2.311e+04 | −50.25 | 1.488e+07 | −3.535e+05 |
| p13 | 1284 | – | −8.966e+04 | 3.009e+04 |
| p14 | – | – | −8870 | −271.7 |
| p20 | −4.752e+06 | −9.431e+04 | −1.376e+07 | 1.716e+08 |
| p21 | −2.467e+05 | 1.182e+05 | 3.861e+07 | −1.041e+07 |
| p22 | 1.522e+04 | – | −2.333e+07 | 4.9e+05 |
| p23 | – | – | 8.746e+04 | −2.234e+04 |
| p30 | 4.883e+06 | 1.8e+05 | 7.202e+06 | −2.543e+08 |
| p31 | 1.108e+05 | 115.4 | −2.023e+07 | 1.013e+07 |
| p32 | – | – | 1.218e+07 | −2.246e+05 |
| p40 | −1.876e+06 | −553.4 | – | 1.883e+08 |
| p41 | – | – | – | −3.695e+06 |
| p50 | – | – | – | −5.576e+07 |

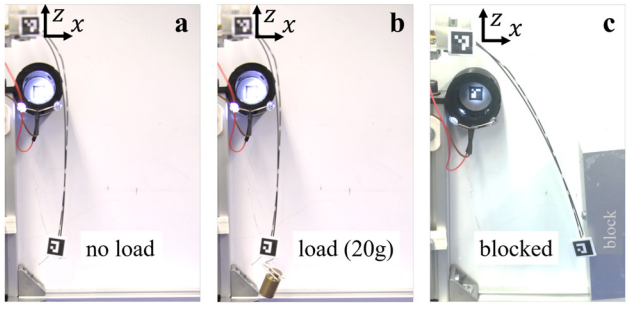


**Figure 8:** Load-heat scenarios for model evaluation with no load (a), 20 g (b) weight, and blocked at 50 % (c).

calculated with the polynomial model using only the measured values of resistance $R$, the vertical force $F_z$, and the heat status as inputs. These estimated values were then compared to the recorded $s_{\text{eval}}$ data. In Figure 10 the fitted 2-dimensional polynomials are shown. The experimental training cycles for fitting the model include electrical resistance $R$ values from 0.62 Ω to 0.7 Ω, loads from 0 g to 100 g and measured deflection values $s$ from −143 mm to −92 mm. Deflection estimations out of these ranges are not valid due to extrapolation errors with high-degree polynomials. Additionally, a comparison of data points of one evaluation trial without load is plotted.

The mean estimation error $\bar{e}_k$ for all data points $k$ in one scenario is defined as

$$\bar{e}_k = \frac{1}{N_{\text{data}}} \sum_{k=1}^{N_{\text{data}}} \underbrace{(|s_{\text{eval}}| - |\hat{s}|)}_{e_k} \tag{4}$$

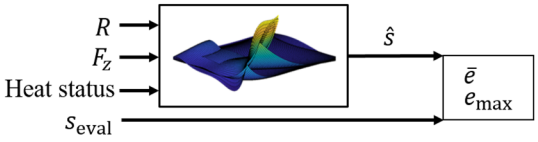


**Figure 9:** Schematic of the evaluation of the polynomial model. Measured deflection data $s_{\text{eval}}$ is collected for 9 scenario-heating cases and compared to the estimated deflection of the model $\hat{s}$ to find the estimation error $e$.

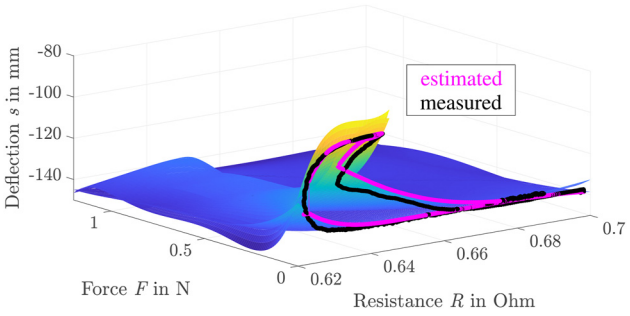


**Figure 10:** Two-dimensional polynomial model for Sections 1–4 correlating resistance $R$ and force $F_z$ in order to find the deflection $s$. Comparing the model's estimation $\hat{s}$ and measured deflection $s_{\text{eval}}$ for 12 s heating time and without load.

where the maximum error is $e_{\max} = \max(e_k)$. The mean estimation error $\bar{e}$ about all evaluation trials is

$$\bar{e} = \frac{1}{N_{\text{trial}}} \sum_{r=1}^{N_{\text{trial}}} \bar{e}_k. \tag{5}$$

# 3 Results

As mentioned in Section 2.3 the dataset to fit the model consists of 22 experimental cycles, 2 trials for 11 different weights. For the evaluation new trials were carried out with 9 different load-heat scenarios (see Section 2.5).

Figure 11 shows the correlation of electrical resistance $R$, as well as estimated deflection $\hat{s}$ and measured deflection $s_{\text{eval}}$ for the 9 load-heat scenarios, with Table 2 summarizing the mean estimation error $\bar{e}$ and maximum estimation error $e_{\max}$.

Overall, $\bar{e}$ is found in a range of 0.17 mm–3.61 mm, and $e_{\max}$ in a range of 4.19 mm–20.78 mm, respectively. The load-heat scenario of 20 g for 4.5 s heating period obtained the smallest estimation error $\bar{e} = 1.23$ mm and $e_{\max} = 4.19$ mm.

Figure 11a–c present each a full actuation cycle including Sections 1–4. For the unloaded case (Figure 11a), a deflection range of up to 44 mm was measured and estimated with a mean error of $\bar{e} = 0.21$ mm. The largest deviation occurred during the transition between Sections 1 and 2 ($e_{\max} = 5.94$ mm). For the loaded case of 20 g (Figure 11b),

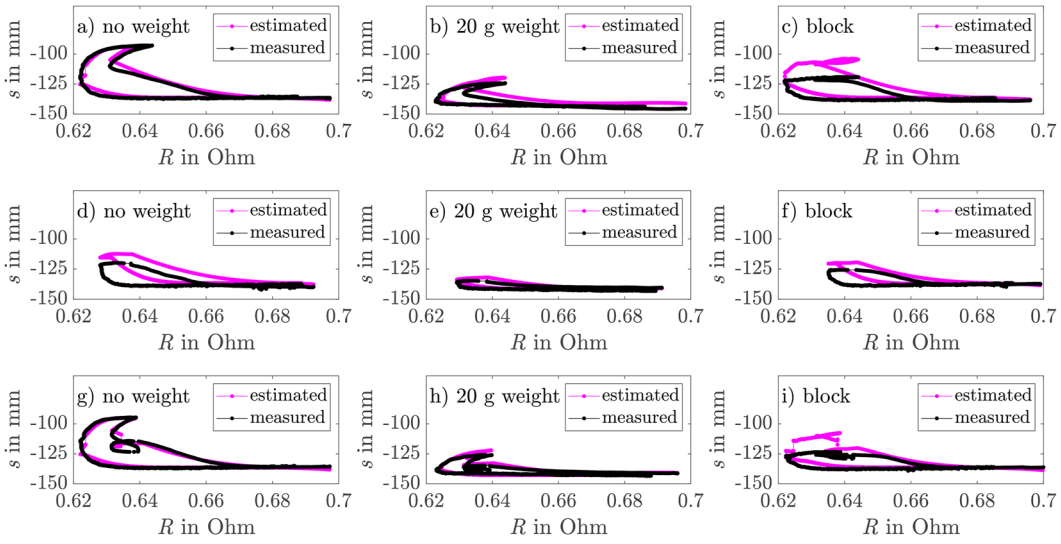


**Figure 11:** Evaluation results of the polynomial model for 9 exemplary load-heat scenarios. Comparing mean estimated deflection $\hat{s}$ to mean measured deflection $s_{\text{eval}}$ for 3 different load cases and heating cases for 12 s (a–c), 4.5 s (d–f) and 4.5 s & 6 s (g–i).

**Table 2:** Results of the model evaluation. Absolute mean and maximum estimation errors for 9 load-heat scenarios. Color-coded from lowest error (green) to highest error (red).

| | | 0 g | 20 g | blocked |
|---|---|---|---|---|
| | $\bar{e}$ | 0.21 mm | 0.88 mm | 2.78 mm |
| **12 s heating** | $e_{\max}$ | 5.94 mm | 6.12 mm | 16.03 mm |
| | $\bar{e}$ | 3.61 mm | 1.23 mm | 1.97 mm |
| **4.5 s heating** | $e_{\max}$ | 20.78 mm | 4.19 mm | 15.35 mm |
| **4.5 s and** | $\bar{e}$ | 0.33 mm | 0.17 mm | 2.03 mm |
| **6 s heating** | $e_{\max}$ | 14.4 mm | 9.33 mm | 16.36 mm |

the deflection was reduced to a range of approximately 20 mm, while the mean estimation error increased to 0.88 mm and the maximum error decreased to 6.12 mm compared to no load. As presumed, the possible deflection decreases with increasing load.

If the deflection is blocked entirely (Figure 11c), Sections 2 and 3 are forced on a similar deflection plateau. The estimation for those sections is shifted toward larger absolute deflections, leading to a mean error $\bar{e} = 2.78$ mm ($e_{\max} = 16.03$ mm). Similarly high errors are observed with all blocking scenarios (cp. Figure 11f and i). We hypothesize that the observed phenomenon and the associated high estimation errors are attributed to the force impact and direction upon the actuator's contact with the block, where the maximum force components measure $|F_x| = 0.1$ N and $|F_z| = 0.04$ N. However, the model's training data only accounts for the $z$ component, relevant in prior actuation cycles with given weights. Consequently, in this particular scenario, wherein $F_x$ dominates, the model appears insufficient to accurately predict the deflection. We intend to address this limitation in our future work.

Figure 11d–f present each only partial actuation cycles with a limited heating period of 4.5 s. Due to the shortened heating the model does not estimate the deflection using Sections 2 and 3. Figure 11d shows that the model estimates the deflection not as low as it was measured. This leads to the largest maximum estimation error $e_{\max}$ of 20.78 mm. A similar behavior occurs in Figure 11f with block and limited heating period of 4.5 s.

In comparison, Figure 11g–i display an extra loop between Sections 2 and 3 where the intermediate cooling period interrupts the heating.

## 4 Discussion

The results of the experimental evaluation suggest that our model is able to predict deflections under certain boundary conditions such as constant ambient temperature and defined load cases.

Still, the model seems to be insufficient to estimate the deflection during shortened heating phases. We hypothesize that this might be due to the lack of training data for such cases.

It should be noted that we only investigated one very simple wire geometry with a history of training cycles ($n > 300$) in this first proof-of-concept. SMA material is highly nonlinear [18] and its actuation behavior depends on its unique history of temperature and load. Therefore, the presented polynomial model in its current form might be

capable to estimate the behavior of this one actuator. However, it might not be able to estimate the characteristics of another actuator with different specifications (e.g. material composition, length, diameter) and history. The transfer to more complex, e.g. S-shaped actuator geometries, is also still pending.

Moreover, the disadvantage of modeling with polynomials becomes apparent in the marginal ranges of the electrical resistance and force values. If a measured value is processed that lies outside the fitting area of $0.62\,\Omega < R < 0.7\,\Omega$ and $0\,\mathrm{N} < F_z < 1.2\,\mathrm{N}$, respectively, the polynomials may tend towards $\pm\infty$ and estimate deflections accordingly.

In order to estimate the shape for unknown load cases, additional force sensors must be used. Adding an additional conventional sensor modality clearly weakens the efficiency of the self-sensing approach. Yet in the context of hand-held instruments in MIS, cost-effective and compact multi-axial force sensors can be integrated easily in the handle design to enhance the instrument.

It should be also noted that the observed maximum wire temperature ($\approx 80\,^{\circ}\mathrm{C}$) is not suitable for an instrument outer surface in direct contact with human tissue. Thus, shape memory alloy compositions with lower austenite finish temperatures should be considered.

For future work, we plan to investigate multiple actuators for large-scale data acquisition and evaluation tests on new, unseen actuators. This would allow for a more comprehensive understanding of their behavior and performance. However, a major challenge is the problem of individual history of each actuator, which remains a limiting factor for efficient data acquisition and poses high demands on the shape-setting process.

On the modeling, further nonlinear modeling approaches could be explored. By incorporating nonlinearities (e.g., Preisach modeling), the behavior and dynamics of the actuator could be estimated more accurately. Additionally, machine learning algorithms (e.g., reinforcement learning) could be employed to identify patterns in the behavior of the actuator and provide a more precise representation of its dynamics. Finally, the integration of these models into closed-loop control could lead to independence from visual support, at least for short periods of time.

# 5 Conclusions

The approach of self-sensing has the potential to enable non-visual tracking of complex two-dimensional shape changes in SMA-driven flexible instruments for medical applications. In this work, we presented a proof-of-concept for a simplified actuator. However, it may be necessary to supplement this approach with additional force sensing capability to safely use it in procedures where interaction forces with human tissue are unknown. Augmenting information of flexible instruments with additional shape information during usage could then compensate for impaired visibility and make minimally invasive procedures safer in the future.

**Author contributions:** All the authors have accepted responsibility for the entire content of this submitted manuscript and approved submission.
**Research funding:** None declared.
**Conflict of interest statement:** The authors declare no conflicts of interest regarding this article.

# References

[1] W. W. G. Ee, W. L. J. Lau, W. Yeo, Y. Von Bing, and W. M. Yue, “Does minimally invasive surgery have a lower risk of surgical site infections compared with open spinal surgery?” *Clin. Orthop. Relat. Res.*, vol. 472, no. 6, pp. 1718—1724, 2014.

[2] K. Mohiuddin and S. J. Swanson, “Maximizing the benefit of minimally invasive surgery,” *J. Surg. Oncol.*, vol. 108, no. 5, pp. 315—319, 2013.

[3] M. R. Abdul Kadir, D. E. O. Dewi, M. N. Jamaludin, M. Nafea, and M. S. Mohamed Ali, “A multi-segmented shape memory alloy-based actuator system for endoscopic applications,” *Sens. Actuators, A*, vol. 296, pp. 92—100, 2019.

[4] A. Syed, Z. T. H. Agasbal, T. Melligeri, and B. Gudur, “Flex sensor based robotic arm controller using micro controller,” *J. Softw. Eng. Appl.*, vol. 05, no. 05, pp. 364—366, 2012.

[5] V. Mishra, N. Singh, U. Tiwari, and P. Kapur, “Fiber grating sensors in medicine: current and emerging applications,” *Sens. Actuators, A*, vol. 167, no. 2, pp. 279—290, 2011.

[6] B. Han, S. Ding, and X. Yu, “Intrinsic self-sensing concrete and structures: a review,” *Measurement*, vol. 59, pp. 110—128, 2015.

[7] K. Ikuta, “Micro/miniature shape memory alloy actuator,” *IEEE Int. Conf. Robot. Autom. Proc.*, vol. 3, pp. 2156—2161, 1990.

[8] J. Prechtl, S. Seelecke, P. Motzki, and G. Rizzello, “Self-Sensing Control of Antagonistic SMA Actuators Based on Resistance-Displacement Hysteresis Compensation,” in *Proceedings of the ASME 2020 Conference on Smart Materials, Adaptive Structures and Intelligent Systems. ASME 2020 Conference on Smart Materials, Adaptive Structures and Intelligent Systems. Virtual, Online. September 15, 2020. V001T03A001.*, ASME, 2020.

[9] M. Kaiser, N. Neblung, and M. Gurka. “Implementation and Investigation of a Compact, Powerful System for Diagnosis and Control of Shape Memory Alloys in Technical Applications.” in *Proceedings of the ASME 2019 Conference on Smart Materials, Adaptive Structures and Intelligent Systems. ASME 2019 Conference on Smart Materials, Adaptive Structures and Intelligent Systems. September 9—11, 2019*. V001T04A004., ASME, 2019.

[10] N. Ma, G. Song, and H.-J. Lee, “Position control of shape memory alloy actuators with internal electrical resistance feedback using

neural networks," *Smart Mater. Struct.*, vol. 13, no. 4, pp. 777—783, 2004.
[11] W. Wang, Y. Tang, and C. Li, "Controlling bending deformation of a shape memory alloy-based soft planar gripper to grip deformable objects," *Int. J. Mech. Sci.*, vol. 193, p. 106181, 2021.
[12] C.-C. Lan and C.-H. Fan, "An accurate self-sensing method for the control of shape memory alloy actuated flexures," *Sens. Actuators, A*, vol. 163, no. 1, pp. 323—332, 2010.
[13] C.-C. Lan, C.-M. Lin, and C.-H. Fan, "A self-sensing microgripper module with wide handling ranges," *IEEE/ASME Trans. Mechatron.*, vol. 16, no. 1, pp. 141—150, 2011.
[14] R. Stalmans, J. V. Humbeeck, and L. Delaey, "The two way memory effect in copper-based shape memory alloys — thermodynamics and mechanisms," *Acta Metall. Mater.*, vol. 40, no. 11, pp. 2921—2931, 1992.
[15] C. Haberland and M. H. Elahinia, "Fabricating NiTi SMA components," in *Shape Memory Alloy Actuators: Design, Fabrication and Experimental Evaluation*, 2015, pp. 191—238.
[16] D. Tarniţă, D. Tarniţă, N. G. Bîzdoaca, I. Mîndrilă, and M. Vasilescu, "Properties and medical applications of shape memory alloys," *Rom J Morphol Embryol*, vol. 50, no. 1, pp. 15—21, 2009.
[17] H. Scherngell and A. Kneissl, "Training and stability of the intrinsic two-way shape memory effect in ni-ti alloys," *Scr. Mater.*, vol. 39, no. 2, pp. 205—212, 1998.
[18] D. K. Soother, J. Daudpoto, and B. S. Chowdhry, "Challenges for practical applications of shape memory alloy actuators," *Mater. Res. Express*, vol. 7, no. 7, p. 073001, 2020.

# Bionotes

**Nikola Fischer**
Institute for Anthropomatics and Robotics (IAR) at Karlsruhe Institute of Technology (KIT), 76131 Karlsruhe, Germany
**nikola.fischer@kit.edu**
**https://orcid.org/0000-0001-9364-3328**

Nikola Fischer is a doctoral candidate at the Karlsruhe Institute of Technology (KIT) at the department for Pervasive Computing Systems (TECO). Before joining KIT in 2020, he was a research assistant at the Hamlyn Centre for Robotic Surgery at Imperial College London. He received his B.Eng. in Mechanical Engineering at the University of Applied Sciences Karlsruhe (HKA) in 2017 and his M.Sc. in Mechatronic and Micro-Mechatronic Systems at HKA and École Nationale Supérieur de Mécanique et des Microtechniques in Besançon, France in 2019. His current research concerns the application of smart materials in the field of health robotics.

**Johannes Knapp**
Institute for Anthropomatics and Robotics (IAR) at Karlsruhe Institute of Technology (KIT), 76131 Karlsruhe, Germany
**johannes.knapp@kit.edu**

Johannes Knapp is an research assistant at the Department of Mobile Machines at the Institute of Vehicle System Technology at the Karlsruhe Institute of Technology (KIT). He obtained his B.Sc. and M.Sc. degrees in mechatronics and information technology in 2019 and 2022 at KIT, with special focus on modelling of shape memory alloys. His current research focus is the development of novel control systems in agricultural machines.

**Franziska Mathis-Ullrich**
Department Artificial Intelligence in Biomedical Engineering (AIBE) at Friedrich-Alexander University Erlangen-Nürnberg (FAU), 91052 Erlangen, Germany
**franziska.mathis-ullrich@fau.de**

Franziska Mathis-Ullrich is professor for surgical robotics at the Friedrich-Alexander-University Erlangen-Nürnberg (FAU) at the Dep. Artificial Intelligence in Biomedical Engineering.Before joining FAU in 2023, she was assistant professor at the Karlsruhe Institute of Technology (KIT) since 2019. Her primary research focus is on minimally invasive and cognition controlled robotic systems and embedded machine learning with emphasis on applications in surgery. She received her B.Sc. and M.Sc. degrees in mechanical engineering and robotics in 2009 and 2012 and obtained her Ph.D. in 2017 in Microrobotics from ETH Zurich, respectively.